Design and Analysis of Novel Bandpass Filters with Adjustable Center Frequency and Bandwidth

Morteza KHAJAVI, Ebrahim FARSHIDI, Mohammad SOROOSH, Shahrzad AJABI*

Dept. of Electrical Engineering, Faculty of Engineering, Shahid Chamran University of Ahvaz, Ahvaz, Iran

mo-khajavi@stu.scu.ac.ir, farshidi@scu.ac.ir, m.soroosh@scu.ac.ir, ajabi_shz@scu.ac.ir

Submitted January 30, 2026 / Accepted May 22, 2026 / Online first June 22, 2026

Abstract. *This paper presents a novel design of microstrip bandpass filters combining stepped-impedance resonators (SIR). Initially, a stepped-impedance resonator is considered as the basic structure, and then the basic design is progressively modified and improved. These enhancements include adding resonators to the basic structure, modifying their dimensions, fundamentally changing their arrangement and connections, and creating air gaps between resonators. These modifications result in significant changes in the frequency response characteristics, shifting the center frequency of the basic model to the X-band. Subsequent steps focus on improving filter parameters such as bandwidth, insertion loss, and return loss, ultimately leading to a dual-band bandpass filter. The single-band filter proposed in this paper has a center frequency of 9 GHz, a bandwidth of 1.83 GHz, an insertion loss of 1.7 dB, and a return loss of 54.6 dB. The dual-band bandpass filter features center frequencies of 7.4 GHz and 10.7 GHz, with bandwidths of 110 MHz and 530 MHz, insertion losses of 1.4 dB and 2.3 dB, and return losses of 22.4 dB and 31.1 dB, respectively. The designed filters are characterized by compact size, high integration, low insertion and return losses, and wide bandwidth. A good agreement is observed between the measured results of the fabricated sample and the simulation results.*

Keywords

Bandpass filter, microstrip, SIR resonator, air gap, insertion loss, return loss

1. Introduction

In recent years, the use of microstrip bandpass filters has gained significant importance due to their numerous advantages, including cost reduction, size reduction, high efficiency, decreased frequency interference, and enhanced security of wireless communication systems [1]. Recent research has focused on the use of various resonators in designing advanced frequency structures. One notable example is the implementation of circular split-ring resonators (CL-SIRs) in the central part of the final structure, which allows for selective tuning of the central frequency of the first passband without affecting the central frequency of the second passband by altering the dimensions of specific resonators. This progress in electromagnetic engineering and microwave filter design provides significant improvements in the performance of telecommunications and radio systems [1]. In [2], the use of transmission line resonators, short circuits, and a circular resonator in the middle section of the structure results in a dual-band frequency response with appropriate insertion and return losses. Additionally, suitable isolation between the first and second passbands is a desirable feature of the final structure. In [3], a design approach for a compact on-chip millimeter wave (mm-wave) dual-passband filter employing hybrid electromagnetic coupling (HEMC) and tunable transmission zeroes (TZs) is presented in a 0.13-μm SiGe BiCMOS technology. This article presents a compact-size tunable wideband bandpass filter (BPF) design that can operate in the S/C band. A hybrid approach combining lumped capacitors and the substrate-integrated waveguide (SIW) technique is chosen [4].

In [5], the proposed design of a dual-band bandpass filter (BPF) is accomplished using two pairs of parallel coupled lines and two open-ended stepped impedance (SIOCS) connections. SIOCS is used to improve selectivity and increase the number of transmission zeroes/poles. In [6], a differential dual-band bandpass filter (DDBBPF) is proposed. In another design example, the implementation of three inverted microstrip gap-waveguide (IM-GWG) bandpass filters for the Ka-band are proposed [7]. Additionally, in [8], the proposed dual-band bandpass filter (BPF) consists of a set of asymmetrical short-circuited resonators (a-SSLRs) and microstrip to balanced slot transmission line structures (MSTSs). In another design example, two flag-shaped resonators combined with two stepped impedance resonators with a coupling system are used to initially enhance the filter's quality response and secondly to add an independent tunability feature to the filter. The final filter has two passbands at central frequencies of 4.42 GHz and 7.2 GHz [9]. Additionally, with the expansion of various communication systems and the rapid development of wireless communication technologies, frequency spectrum resources have become increasingly scarce and important. Therefore, with the rising demand

DOI: 10.13164/re.2026.0335

for wireless communication systems and the necessity to simultaneously support two or more frequency bands, dual or multi-band frequency systems, which can respond to two or more frequency bands at the same time, have become hot research topics in this field and have attracted considerable attention. Among these systems, dual-band microstrip bandpass filters (DBBPF) are noteworthy as a crucial passive component in wireless communications, extensively studied and developed.

Given the current trend in multi-band communication systems, the application of balanced circuits in the design of multi-band components, especially filters that play a vital role in the performance of these systems, has significantly increased. This advancement aims to improve efficiency and increase bandwidth in modern communication networks [10], [11]. In [12], a compact dual-band bandpass filter with flexibility and independence from differential mode response is presented. The filtering mechanism of this structure is based on the use of embedded magnetic resonators. This provides two advantages: a high level of miniaturization and two differential passbands that can be independently tuned. In [13], a new type of stepped impedance resonator is proposed for the design of a dual-band bandpass filter. Furthermore, compact multi-band filters with applications in GSM, WiMAX, and WLAN systems are presented. The design is based on the specifications of interdigital capacitive resonators and stepped impedance with overlapping cross-coupling structures. Despite the dual-band nature of the structures and the use of diverse resonators in the proposed designs, the need for tunability and improved frequency response persists. Consequently, employing innovative design methodologies and optimizing the utilization of various resonator types is essential to achieve optimal frequency characteristics [14, 15, 16].

In this paper, a simple yet systematic design approach is presented that can adequately address all (or most) of the critical features required for dual-band bandpass filters (BPFs). The techniques employed in the design of the dual-band bandpass filter include the use of a gap, transmission lines, intermediate stubs, and the adjustment of the dimensions of each of the mentioned resonators in the proposed filter structure. These techniques are utilized to achieve a suitable structure along with an ideal frequency response for the final filter. Therefore, by using stepped impedance resonators and creating a symmetrical structure with an air gap between them, satisfactory results have been obtained. Furthermore, a circuit model is provided, and the results of this model are compared with the frequency response of the designed filter to evaluate the proposed structure. Continuing this research, Step 2 describes the basic principles for designing circuit models. Step 3 considers the design methodology of the single-band bandpass filter, its circuit model design, and the feasibility of tuning its bandwidth. Step 4 evaluates the dual-band bandpass filter structure, its circuit model, and the tunability of the center frequency of the passbands. Finally, Step 5 describes and compares the measurement results of the fabricated prototypes and the simulation results.

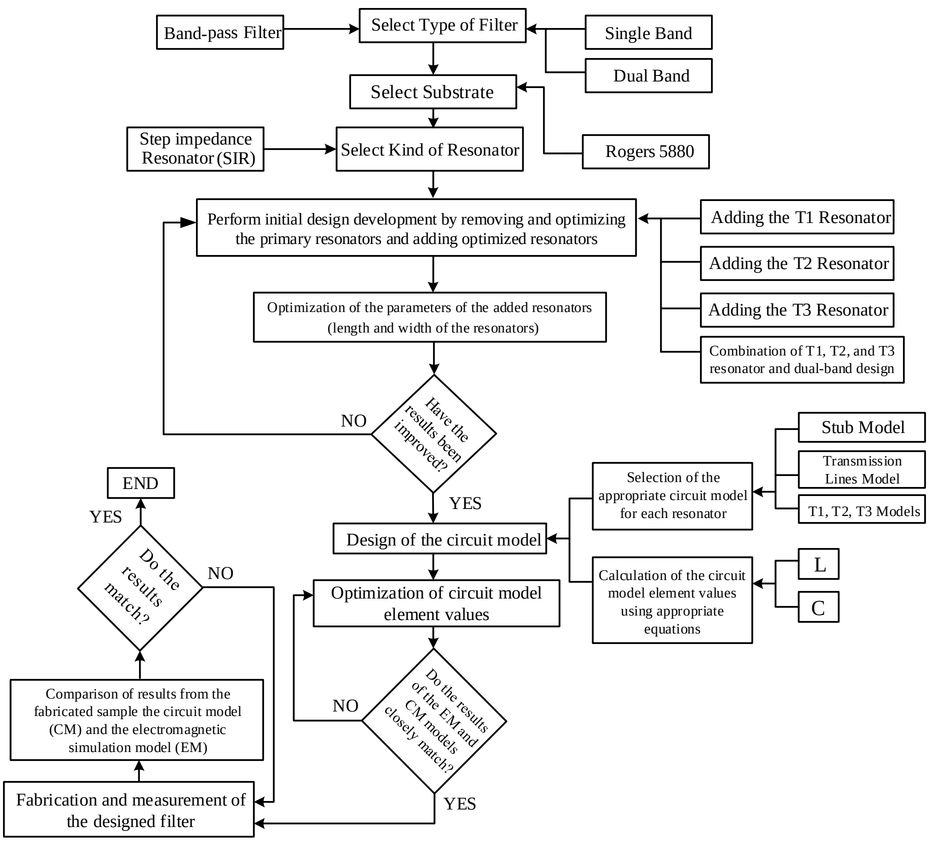

Fig. 1. Flowchart of the design process for microstrip bandpass filters.

2. Basic Principle

To conduct a more detailed examination of the proposed basic model, the steps for designing the equivalent circuit model of various components of the basic design are presented below. As shown in Fig. 1, the step-by-step comprehensive design process of the filters presented in this study is provided in the form of a flowchart.

3. Equivalent Circuit Model of the Air Gap

Here, the circuit equivalence of the air gap between the two vertical stubs used in the design of the middle section of the basic model is presented. Therefore, in the equivalent compact circuit, a series gap structure can be utilized (Fig. 2).

As shown in Fig. 2(a), there is a significant capacitive effect along the gap, denoted as C_g. The capacitors connected to ground, C_p, represent the edge fields radiated from both ends of the line in the symmetrical gap. Based on the three physical parameters consisting of the air gap spacing (s), length (h), and width (W), as illustrated in Fig. 2(a), the capacitance values can be calculated using the expressions provided in [17] as follows:

$$C_p = 0.5C_e \quad \text{and} \quad C_g = 0.5C_o - 0.25C_e \tag{1a}$$

in which

$$C_o = W\left(\frac{\varepsilon_r}{9.6}\right)^{0.8}\left(\frac{s}{W}\right)^{m_o}\exp(k_o), \tag{1b}$$

$$C_e = 12W\left(\frac{\varepsilon_r}{9.6}\right)^{0.9}\left(\frac{s}{W}\right)^{m_e}\exp(k_e). \tag{1c}$$

According to (1b), (1c), the computational relations for variables in these equations are categorized and computed as follows based on the s/W ratio [17]:

$$\begin{aligned} m_o &= \frac{W}{h}\left[0.619\log\left(\frac{W}{h}\right) - 0.3853\right], \\ k_o &= 4.26 - 1.453\log\left(\frac{W}{h}\right), \end{aligned} \quad \text{for } 0.1 \le \frac{s}{W} \tag{2a}$$

$$m_e = 0.8675, \quad k_e = 2.0439\left(\frac{W}{h}\right)^{0.12} \quad \text{for } 0.1 \le \frac{s}{W} \le 0.3, \tag{2b}$$

$$m_e = \frac{1.565}{\left(\frac{W}{h}\right)^{0.16}} - 1, \quad k_e = 1.97 - \frac{0.03}{\frac{W}{h}} \quad \text{for } 0.3 \le \frac{s}{W} \le 1. \tag{2c}$$

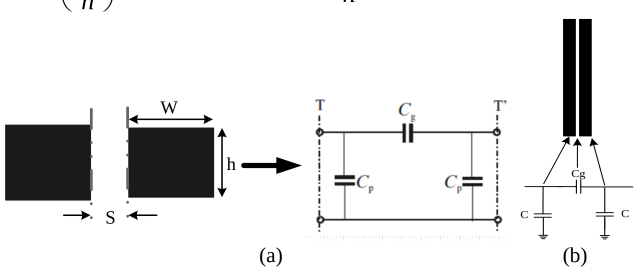

Fig. 2. (a) Air gap and equivalent capacitor. (b) Open-circuit resonators with the air gap between them and their equivalent circuit [17].

4. Equivalent Circuit Model of Transmission Line and Stubs

In general, the characteristics of microstrip transmission lines are expressed by the effective dielectric constant $\varepsilon_{\text{reff}}$ and the characteristic impedance Z_c [17]:

$$\varepsilon_{\text{reff}} = \frac{C_d}{C_a}, \quad Z_c = \frac{1}{c\sqrt{C_d C_a}}$$

in which

$$C_a = \frac{2\pi\varepsilon_0}{\ln\left(\frac{8h}{W} + \frac{W}{4h}\right)} \quad \text{for } \frac{W}{h} \le 1$$
$$C_a = \varepsilon_0\left(\frac{W}{h} + 1.393 + 0.667\ln\left(\frac{W}{h} + 1.444\right)\right) \quad \text{for } \frac{W}{h} \ge 1 \tag{3a}$$

where W is the width of the microstrip line, l is the length of the microstrip line, h is the thickness of the substrate, c is the speed of light in free space, C_a is the capacitance per unit length due to the dielectric substrate, and C_d is the capacitance from which the values of the circuit model elements such as inductors and capacitors can be obtained using (3a). Equation (3b), (3c) for $\varepsilon_{\text{reff}}$ and Z_c is as follows [17]:

$$\begin{aligned} \varepsilon_{\text{reff}} &= \frac{\varepsilon_r + 1}{2} + \frac{\varepsilon_r - 1}{2}\left\{\left(1 + 12\frac{h}{W}\right)^{-0.5} + 0.04\left(1 - 1\frac{h}{W}\right)^2\right\}, \\ Z_c &= \frac{\eta}{2\pi\sqrt{\varepsilon_{\text{reff}}}}\ln\left(8\frac{h}{W} + 0.25\frac{W}{h}\right), \end{aligned} \quad \text{for } \frac{W}{h} \le 1, \tag{3b}$$

$$\begin{aligned} \varepsilon_{\text{reff}} &= \frac{\varepsilon_r + 1}{2} + \frac{\varepsilon_r - 1}{2}\left\{\left(1 + 12\frac{h}{W}\right)^{-0.5}\right\}, \\ Z_c &= \frac{\eta}{2\pi\sqrt{\varepsilon_{\text{reff}}}}\ln\left(8\frac{h}{W} + 0.25\frac{W}{h}\right), \end{aligned} \quad \text{for } \frac{W}{h} \ge 1. \tag{3c}$$

where $\eta = 120\pi\ \Omega$ is the wave impedance in free space and ε_r is the relative permittivity of the substrate before the effect of the resonator layers. Now, the relationships can be summarized in the following form [17]:

$$Z_c = \frac{120\pi}{\frac{C_a}{\varepsilon_0}\sqrt{\varepsilon_{\text{reff}}}}, \quad V_p = \frac{c}{\sqrt{\varepsilon_{\text{reff}}}}, \tag{4a}$$

$$L_{\text{stub}} = \frac{Z_c l}{V_p}, \quad c = \frac{l}{Z_c V_p}. \tag{4b}$$

In (4a), parameter V_p is the phase velocity, which is obtained from the following (5a), (5b). λ_g is the guided wavelength, ε_0 is the permittivity of free space, and β is the propagation constant [17].

$$V_p = \frac{\omega}{\beta} = \frac{c}{\sqrt{\varepsilon_{\text{reff}}}}, \quad \beta = \frac{2\pi}{\lambda_g}, \tag{5a}$$

$$\lambda_g = \frac{\lambda_0}{\sqrt{\varepsilon_{\text{reff}}}} = \frac{300}{f\sqrt{\varepsilon_{\text{reff}}}} \text{ (mm) and } f \text{ (frequency, GHz).} \tag{5b}$$

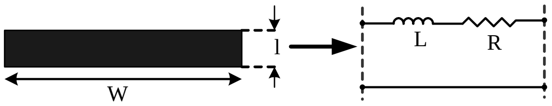

Fig. 3. High impedance straight line and its equivalent circuit [17].

5. Structure of the Line

Figure 3 shows a narrow conductor transmission line of length l and width W, which is equivalent to an inductor and a small series resistance. The inductance can be calculated using (6a) [5], [17]:

$$L_{\text{TransmissionLine}}(\text{nH}) = 2\times10^{-4} l\left[\ln\left(\frac{l}{W+l}\right)+1.193+0.223\frac{W}{l}\right]K_{\text{g}} \tag{6a}$$

with l (mm) and $K_g = 0.57 - 0.145\ \ln(w/h)$, for $w/h > 0.05$, is the ground-plane influence coefficient (h is the thickness of the dielectric substrate).

6. Single-Band Bandpass Filter Design

Initially, a basic structure with a frequency response similar to a bandpass filter has been obtained using stepped impedance resonators. The basic resonator structure is designed using a standard λ/4 resonator and stepped impedance resonator (SIR) topology, which consists of a combination of transmission lines and stubs arranged in an H shape. As shown in Fig. 4, the basic structure is presented. The designed basic structure includes a transmission line in the middle of the structure and two stubs on the sides, and the structure is designed to be symmetrical. The basic structure has one passband at frequency of 16.4 GHz; however, it is distant from the target structure of this paper in terms of frequency response characteristics. Therefore, it is necessary to make modifications to the structure to change the central frequency, improve insertion and return losses, and ultimately increase the bandwidth. This enhancement of the structure will be carried out step by step.

As shown in Fig. 5, the main design structure has undergone fundamental changes. In the modified structure, the open-ended stubs that were located on the left and right sides of the structure have been moved to the middle section after adjustments to their dimensions. Following this relocation, an air gap has been created between the two stubs in the middle of the structure. Additionally, the dimensions of the transmission lines in the modified structure have also changed, as indicated in Fig. 5. Another significant change is the addition of two T1 resonators to the middle stubs at the upper and lower sides of the structure. With the total changes applied, the frequency response has undergone substantial alterations, shifting the central frequency to the X-band and converting the frequency response to a single band. Furthermore, the bandwidth has improved significantly. However, as shown in Fig. 5(b), the return loss and insertion loss are 9.2 dB and 0.6 dB, respectively, indicating a need for further improvements in losses through modifications to the structure. The precise dimensions of the improved structure are presented in Tab. 1.

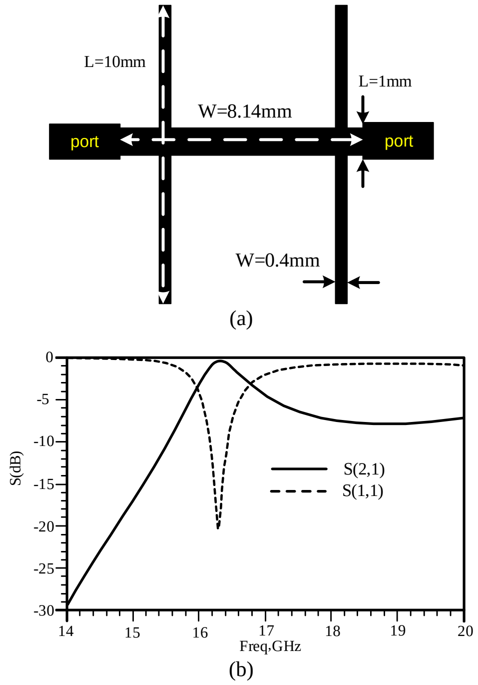

Fig. 4. (a) Basic structure. (b) The frequency response.

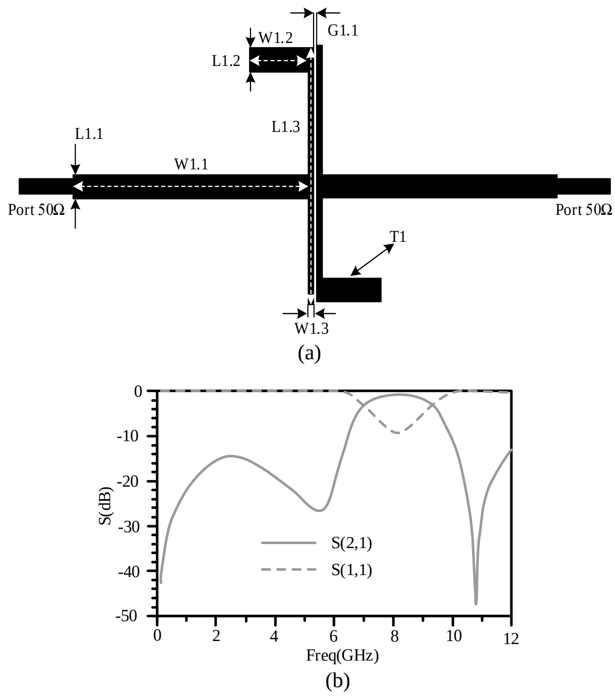

Fig. 5. (a) Basic design structure by adding an air gap (Design 1). (b) Frequency response with additional air gap.

Parameter	Dimension (mm)	Parameter	Dimension (mm)
W1.1	11	L1.1	1
W1.2	2.75	L1.2	1
W1.3	0.24	L1.3	11
G1.1	0.14		

Tab. 1. Dimensions of the modified basic structure.

In Fig. 6(a), the basic design and its circuit model are presented. In the designed model, using equations (1a) to (6a), an appropriate and accurate circuit model corresponding to each of the resonators in the basic structure has been determined and calculated. Finally, a final circuit model for the designed basic structure is presented, and its frequency response is compared with the frequency response of the EM (Electromagnetic model) (see Fig. 6(b)). As evident in Fig. 6(c), the frequency response of the designed circuit model exhibits excellent agreement with the electromagnetic model in terms of key frequency-domain characteristics including insertion loss, return loss, bandwidth, and particularly center frequency. The precise values of these frequency characteristics are provided in Tab. 3.

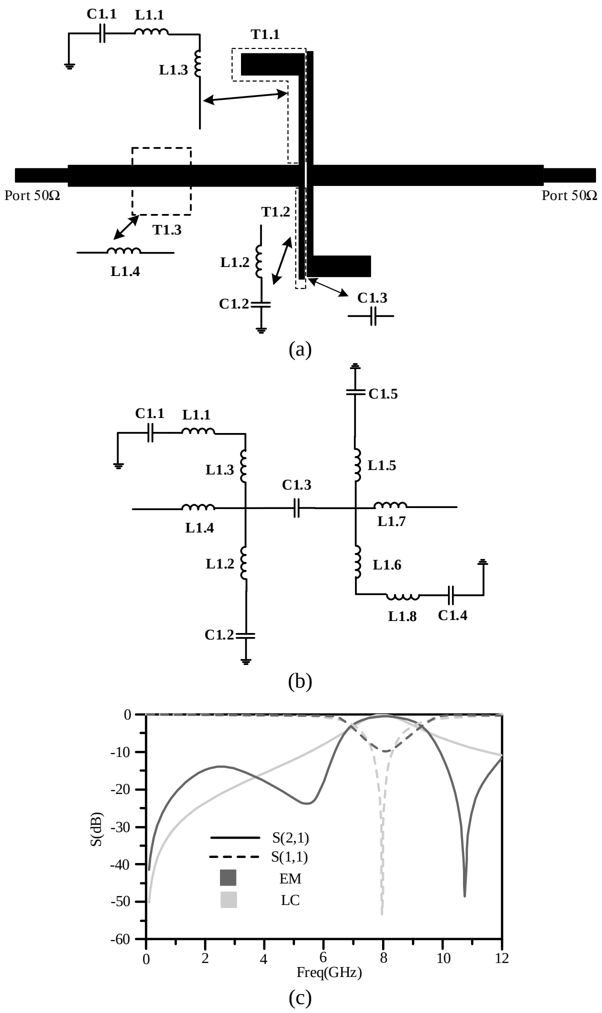

Fig. 6. (a) The basic structure by adding and air gap. (b) Circuit model. (c) Frequency response comparison.

Element	Value	Element	Value
L1.4	4 nH	C1.3	0.050 pF
C1.1	0.0669 pF	C1.5	0.038 pF
L1.1	0.2 nH	L1.5	2.3 nH
L1.3	2.75 nH	L1.7	4 nH
L1.2	1.7 nH	L1.6	2.26 nH
C1.2	0.0403 pF	L1.8	0.2 nH
C1.4	0.0669 pF		

Tab. 2. Values of the circuit model of the basic design.

Model	CF (GHz)	BW (GHz)	RL (dB)	IL (dB)
EM Model	7.9	2.36	9.9	0.59
Circuit Model	7.9	2	52.9	0.005

Tab. 3. Frequency response characteristics (CF – center frequency, RL – return loss, IL – insertion loss).

As shown in Fig. 6(a), the inductor L1.3 and the inductor and capacitor L1.1 and C1.1 represent the equivalent circuit model of the resonators T1.1. The inductor L1.2 and the capacitor C1.2 represent the circuit model of the resonator T1.2. The capacitor C1.3 represents the equivalent circuit model of the air gap between the two middle stubs, and the inductor L1.4 represents the equivalent circuit model of the resonator T1.3. Since the structure is symmetrical, the resonators on the right side of the structure have the same dimensions, and a similar circuit model has been designed for them as on the left. The precise values of the circuit model elements for each of the EM model resonators are provided in Tab. 2. These values have been scanned and refined to achieve a precise match of the frequency characteristics between the electromagnetic model and the designed circuit model, especially for accurately matching the central frequencies. The precise values of the frequency response for the designed circuit model and the EM model are presented in Tab. 3.

In Fig. 7(a), by modifying the dimensions of the resonator T1 and symmetrically adding it to the middle stubs, as well as adjusting the dimensions of the open-ended stubs, a significant improvement in both the insertion loss and return loss is achieved. Specifically, the return loss improves from 9.22 dB to 44 dB, and the insertion loss im-

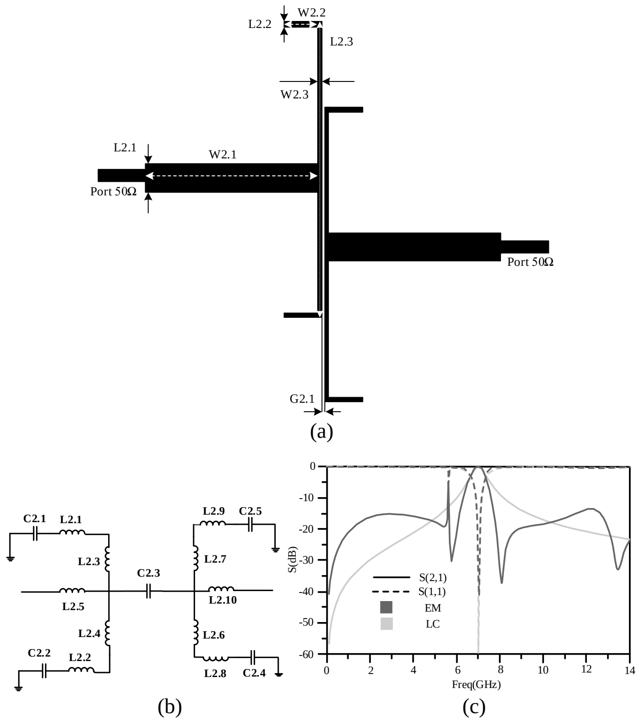

Fig. 7. (a) Altered basic structure (Design 2). (b) Modified basic structure circuit model. (c) Comparison of circuit and EM model frequency response.

Parameter	Dimension (mm)	Parameter	Dimension (mm)
W2.1	9	L2.1	1.5
W2.2	2	L2.2	0.2
W2.3	0.22	L2.3	15
G2.1	0.14		

Tab. 4. Dimensions of the modified basic structure (Design 2).

Element	Value	Element	Value
L2.5	1.77 nH	C2.3	0.15 pF
C2.1	0.392 pF	C2.5	0.392 pF
L2.1	1.5 nH	L2.9	1.5 nH
L2.3	5 nH	L2.7	5 nH
L2.4	5 nH	L2.10	1.77 nH
L2.2	1.5 nH	L2.6	5 nH
C2.2	0.392 pF	L2.8	1.5 nH
C2.4	0.392 pF		

Tab. 5. Values of the circuit model of Design 2.

Model	CF (GHz)	BW (MHz)	RL (dB)	IL (dB)
EM Model	7	680	41.3	0.09
Circuit Model	7	660	59.7	0.03

Tab. 6. Frequency response characteristics.

proves from 0.5 dB to 0.1 dB. However, the central frequency decreases from 8.1 GHz to 6.9 GHz. As shown in Fig. 7(c), with the applied changes, the modified structure has a central frequency of 6.9 GHz, a bandwidth of 680 MHz, an insertion loss of 36.12 dB, and a return loss of 0.1 dB, although it still requires bandwidth improvement. Furthermore, the transmission zeros generated on both sides of the frequency response of the proposed filter result from making the structure asymmetrical, as illustrated in Fig. 6. Accordingly, by introducing asymmetry into the structure during the optimization of the single-band filter design, transmission zeros can be effectively created. With these modifications to the structure, these changes must also be reflected in the calculation of the equivalent circuit model elements of the resonators. The precise dimensions of the improved structure are provided in Tab. 4. The precise values of the circuit model elements for each of the EM model resonators are provided in Tab. 5. These values have been scanned and refined to achieve a precise match of the frequency characteristics between the electromagnetic model and the designed circuit model, especially for accurately matching the central frequencies.

In Fig. 7(c), the frequency response of the circuit model and the designed electromagnetic model is shown and compared with each other. As indicated in Fig. 7(c), the circuit model has values corresponding to those in Tab. 6, which show a good match in terms of central frequency with the electromagnetic model. The precise values of the frequency response for the designed circuit model and the EM model are presented in Tab. 6.

7. Addition of Resonator T2

With the addition of resonator T2 to the middle section of the structure, in addition to shifting the central frequency, the bandwidth also increases. The precise position of the connection of resonator T2 to the middle stub, along with its initial and final dimensions, plays a crucial role in optimizing the insertion loss, return loss, and also increasing the bandwidth by 360 MHz. Specifically, as the width of resonator T2 increases from 0.2 mm to 1.6 mm, the bandwidth increases from 610 MHz to 970 MHz.

In Fig. 8(b), the circuit model of the enhanced structure with resonator T2 is presented. The addition of resonator T2 to the EM model also causes changes in the circuit model. The addition of inductors L3.10, L3.3, and capacitors C3.3, C3.6 in the circuit model corresponds to the addition of resonator T2 to the sides of the middle open-ended stubs. Additionally, depending on which part of the middle stub resonator T2 is added to, the values of inductors L3.7 and L3.5 on the left side of the circuit model and the values of inductors L3.12 and L3.14 on the right side of the circuit model will also change. In Fig. 8(c), the frequency response of the circuit model of the enhanced basic structure after the addition of resonator T2 is compared with the frequency response of the EM model and examined. The frequency response of the circuit model shows a precise match in terms of central frequency and bandwidth with the EM model. The precise dimensions of the improved structure are shown in Tab. 7.

The precise values of the elements of the equivalent circuit model for resonator T2 are presented in Tab. 8. To ensure a proper match between the frequency response of

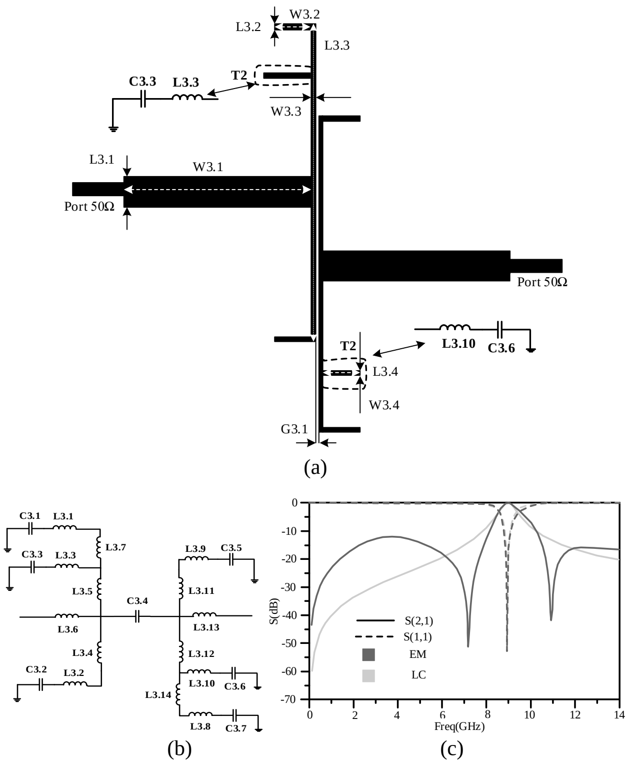

Fig. 8. (a) Basic structure with the addition of a T2 resonator (Design 3). (b) Circuit model of the modified basic structure with the addition of a T2 resonator. (c) Comparison of the frequency response of the circuit and EM model.

Parameter	Dimension (mm)	Parameter	Dimension (mm)
W3.1	5.8	L3.1	1
W3.2	1.3	L3.2	0.13
W3.3	0.15	L3.3	11.76
W3.4	1.3	L3.4	0.16
G3.1	0.13		

Tab. 7. Dimensions of the modified basic structure (Design 3).

Element	Value	Element	Value	Element	Value
L3.6	10 nH	C3.4	0.015 pF	L3.2	0.035 nH
C3.1	0.0062 pF	C3.5	0.0062 pF	C3.2	0.0062 pF
L3.1	0.035 nH	L3.9	0.035 nH	C3.7	0.0062 pF
L3.7	1.18 nH	L3.11	3.05 nH	L3.14	1.21 nH
L3.3	0.044 nH	L3.13	10 nH	L3.8	0.035 nH
C3.3	0.0076 pF	L3.12	2.1 nH		
L3.5	2.12 nH	L3.10	0.044 nH		
L3.4	3.06 nH	C3.6	0.0076 pF		

Tab. 8. Values of the circuit model of the basic design after adding resonator T2.

Model	CF (GHz)	BW (MHz)	RL (dB)	IL (dB)
EM Model	8.9	970	52.6	0.09
Circuit Model	8.9	810	41.9	0.02

Tab. 9. Frequency response characteristics.

the circuit model (CM) and the EM model, the calculated values of the elements have been scanned and improved.

The results of the frequency response for the circuit model and the EM model are presented in Tab. 9.

8. Addition of Resonator T3

As shown in Fig. 9(a), the addition of resonator T3 to the sides of the structure enhances the bandwidth. How resonator T3 is added to the structure is symmetrical. Ultimately, with the addition of resonator T3 to the basic structure in Fig. 9(a), the final single-band filter structure is formed. The exact placement of resonator T3 within the structure, how it connects to the transmission lines on the sides of the structure, and the precise tuning of the dimensions of resonator T3 are crucial factors in enhancing the bandwidth. With the addition of resonator T3, the bandwidth improves from 0.97 GHz to 1.88 GHz, with a central frequency of 9 GHz, an insertion loss of 73.23 dB, and a return loss of 0.03 dB (Fig. 9(c)). Given the changes made to the EM model, the circuit model also undergoes modifications. In Fig. 9(b), the final circuit model, including the equivalent circuit model of resonator T3, is presented.

In the enhanced circuit model, inductors L4.9 and L4.6 and capacitors C4.4 and C4.5 on the left side of the circuit model form the equivalent of resonator T2, while inductors L4.19 and L4.20 and capacitors C4.11 and C4.10 are on the right side. Additionally, based on the location of resonator T3 added to the transmission lines on the sides of the EM model, the values of the equivalent inductors must also be adjusted, such that L4.3 and L4.4 on the left side and inductors L4.15 and L4.17 on the right side will change. The precise dimensions of the improved structure are shown in Tab. 10. Furthermore, at each stage after adding a new resonator, all parameters of each resonator in the structure have been optimized over several steps to achieve the best possible result. The most significant impact of adding the T3 resonator to the designed bandpass filter structure is the very substantial increase in the passband bandwidth. Overall, the evolution of the filter structure from the beginning up to this design stage has been toward increasing the passband bandwidth. This goal has been achieved gradually through the step-by-step addition of the T1, T2, and T3 resonators.

Using relations (3a) to (6a), the precise values of the elements added to the circuit model have been calculated and are presented in Tab. 11. For matching purposes, the fre-

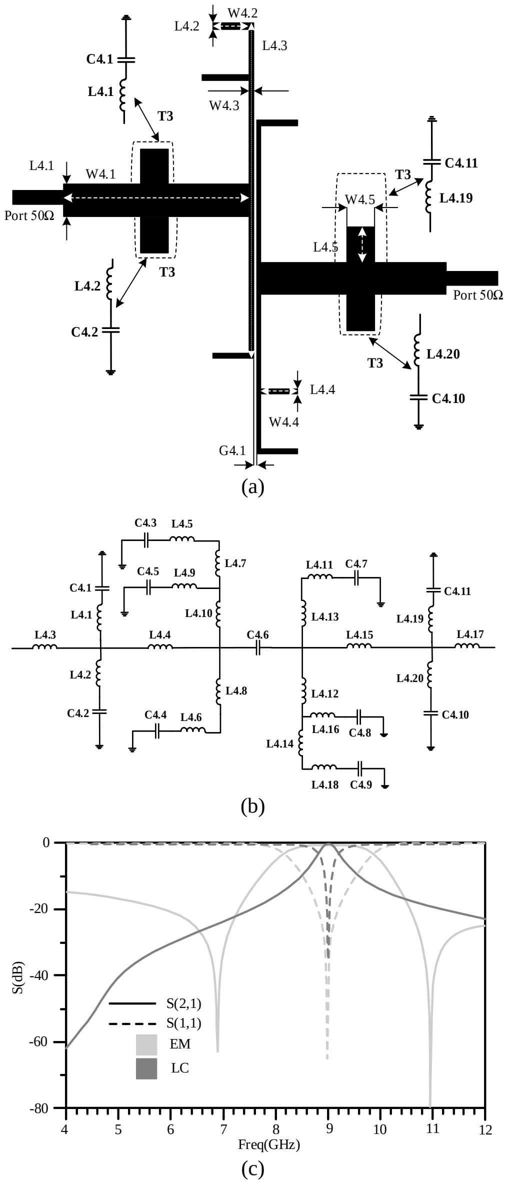

Fig. 9. (a) Basic structure with the addition of a T3 resonator (Design 4). (b) Circuit model of the modified basic structure with the addition of a T3 resonator. (c) Comparison of the frequency response of the circuit and EM model.

Parameter	Dimension (mm)	Parameter	Dimension (mm)
W4.1	5.8 mm	L4.1	1 mm
W4.2	1.3 mm	L4.2	0.13 mm
W4.3	0.15 mm	L4.3	11.76 mm
W4.4	1.3 mm	L4.4	0.16 mm
W4.5	1 mm	L4.5	1 mm
G4.1	0.13 mm		

Tab. 10. Dimensions of the modified basic structure after adding resonator T3 (Design 4).

Element	Value	Element	Value	Element	Value	Element	Value
L4.3	9 nH	C4.6	0.0158 pF	C4.5	0.00763 pF	L4.14	1.21 nH
C4.1	0.023 pF	C4.7	0.0062 pF	L4.7	1.18 nH	L4.18	0.035 nH
L4.1	0.18 nH	L4.11	0.035 nH	L4.5	0.035 nH	C4.9	0.0062 pF
L4.2	0.18 nH	L4.13	3.05 nH	C4.3	0.0062 pF	C4.11	0.023 pF
C4.2	0.023 nH	L4.15	1.67 nH	L4.20	0.18 nH	L4.19	0.18 nH
L4.4	1.67 nH	L4.12	2.1 nH	C4.10	0.023 pF	C4.4	0.0062 pF
L4.10	2.12 nH	L4.16	0.044 nH	L4.8	3.06 nH	L4.6	0.035 nH
L4.9	0.044 nH	C4.8	0.0076 pF	L4.15	1.67 nH	L4.17	9 nH

Tab. 11. Values of the circuit model of the basic design after adding resonator T3.

Model	CF (GHz)	BW (GHz)	RL (dB)	IL (dB)
EM Model	9	1.88	65.4	0.2
Circuit Model	9	0.75	34.9	0.001

Tab. 12. Frequency response characteristics.

quency response of the circuit model (CM) and the EM model has been scanned and improved based on the calculated values of the elements.

In Fig. 9(c), a comparison of the frequency response of the modified circuit model and the frequency response of the EM model is presented. The frequency response of the circuit model shows a precise match in terms of center frequency with the EM model. The results of the frequency response for the circuit model and the EM model are presented in Tab. 12.

9. Examination of Changes in the Single-Band Bandpass Filter Structure Based on the Width Variation of Resonators T2 and T3

With the addition of resonators T2 and T3 to the structure to improve the passband (Fig. 10(a) and (b)), the bandwidth has increased from 610 MHz to 990 MHz and from 1.2 GHz to 1.88 GHz, respectively. It is important to note that the dimensions of these resonators and their connection to the designed structure are very critical.

In Tab. 13, various cases of changing the dimensions of resonator T2 and the impact of these changes on the

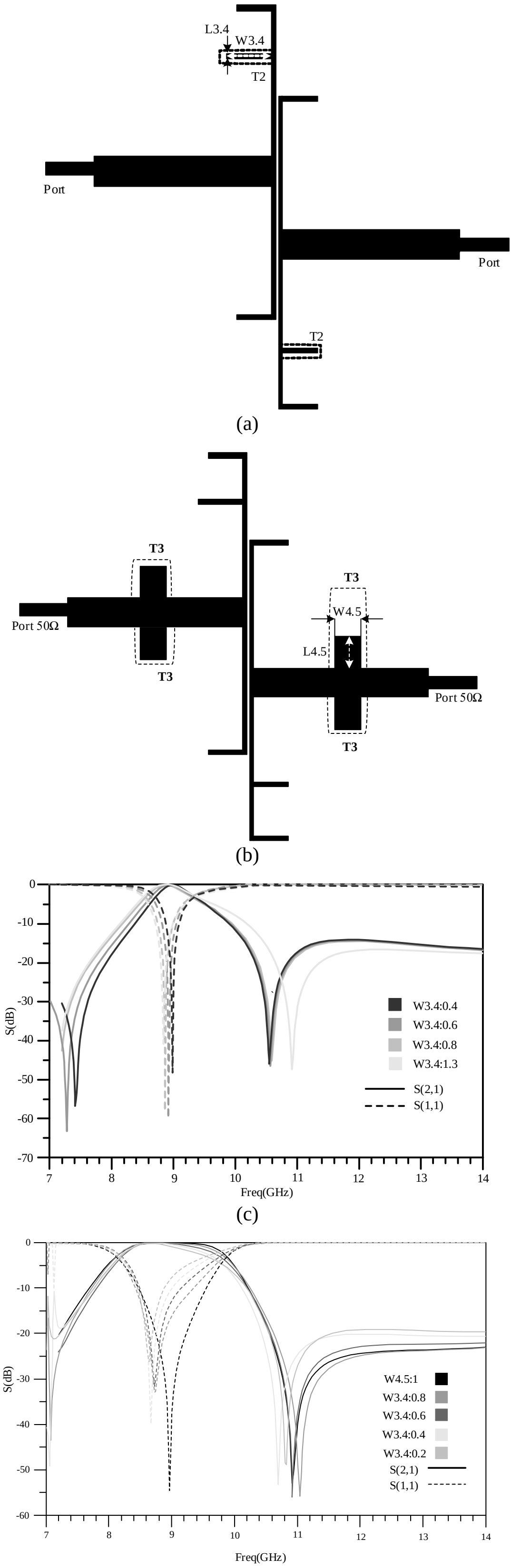

Fig. 10. (a) Basic structure with the addition of T2 resonator. (b) Basic structure with the addition of T3 resonator. (c) Frequency response results of the effect of changing the dimensions of the T2 resonator. (d) Results of the frequency response of the effect of changing the dimensions of the T3 resonator.

Dimensions (mm) (l = 0.16)	CF (GHz)	BW (MHz)	RL (dB)	IL (dB)
W = 0.2	9	610	38.6	0.1
W = 0.4	9	640	59.5	0.1
W = 0.6	8.9	720	41.3	0.1
W = 0.8	8.9	770	50.5	0.1
W = 1	8.8	850	51	0.1
W = 1.2	8.7	920	37.9	0/09
W = 1.3	8.7	990	41	0/09

Tab. 13. Effect of changing T2 resonator dimensional values.

Dimensions (mm) (l = 1)	CF (GHz)	BW (GHz)	RL (dB)	IL (dB)
W = 0.16	8.9	1.2	52.5	0.08
W = 0.2	8.8	1.4	46.9	0.08
W = 0.4	8.7	1.54	47.6	0.06
W = 0.6	8.77	1.63	46.8	0.06
W = 0.8	8.8	1.73	38.7	0.06
W = 1	9	1.88	73.23	0.03

Tab. 14. Effect of changing T3 resonator dimensions.

characteristics of the filter (Fig. 10(a)) are presented. Resonator T2 has the feature that while maintaining desirable values for insertion and return losses, increasing the width of the resonator (W) from 0.2 mm to 1.3 mm, while keeping the height of the resonator (l) constant, results in an increase in the filter's bandwidth by approximately 100 MHz steps. This means that a desired bandwidth between 610 MHz and 990 MHz can be selected without changing other characteristics of the frequency response. In the next step, by adding resonator T3 to the filter structure, the bandwidth is ultimately upgraded from 990 MHz to 1.88 GHz. Table 14 shows the changes in the width of resonator T3 and its effect on the passband. Similar to resonator T2, resonator T3 also has the feature that, while maintaining acceptable insertion and return losses, each time the width of the resonator is changed, a desired bandwidth in the range of 1.2 GHz to 1.88 GHz can be achieved.

As shown in Tab. 14, the width of resonator T3 starts at 0.16 mm and increases by 0.2 mm at each step, resulting in a significant enhancement in bandwidth. Ultimately, at a width of 1 mm, we achieve a bandwidth of 1.88 GHz.

10. Design of a Dual-Band Bandpass Filter

The designs presented up to this stage each have their specific features. In Design 1, by modifying the basic design and adding resonator T1 to the middle section of the structure, as shown in Fig. 5, an excellent bandwidth is achieved. However, despite the desirable bandwidth, the results regarding parameters such as insertion loss and return loss are not satisfactory, necessitating modifications to improve these losses. In Design 2, by adjusting the dimensions of resonator T1 and symmetrically adding the modified resonator T1 to both sides of the middle stubs (Fig. 7), a significant improvement in insertion loss and return loss is achieved. However, despite this improvement, the bandwidth has significantly decreased, and the passband frequency has also shifted. Then, in Design 3, by adding resonator T2 to both sides of the middle stubs (Fig. 8), a very good enhancement in bandwidth is observed, and the insertion loss and return loss are also acceptable. In Design 3, the bandwidth increases to 1 GHz. Finally, in Design 4, by symmetrically adding resonator T3 to both sides of the structure, the bandwidth has significantly increased compared to Design 3. As seen in Fig. 9, the bandwidth has increased to 1.88 GHz. Moreover, there is a good improvement in parameters such as insertion loss and return loss, with values of 0.03 dB for insertion loss and 73.23 dB for return loss, which are very desirable. Overall, the modifications made from Design 1 to Design 4 have led to improvements in the frequency response parameters, including bandwidth, insertion loss, and return loss. Subsequently, considering the demand for dual-band and multi-band systems, a dual-band bandpass filter has been proposed by making modifications to the single-band filter structure and utilizing a combination of designs 1 to 4.

The main design approach after stage 4 is to upgrade the single-band filter to a dual-band filter. This enhancement is achieved during the design process through fundamental modifications made to the single-band filter structure. These modifications consist of altering the air gap spacing in the middle section of the structure and adding a systematic network of transmission lines and stubs. Furthermore, to improve the passband bandwidth, two transmission lines with specific dimensions are attached to the stubs: one at the upper part of the left stub and one at the lower part of the right stub. The ideas employed in the dual-band filter design stages, such as connecting transmission lines to stubs with specific spacing to improve frequency characteristics, were effectively implemented during the four design stages of the single-band filter and are also well utilized in the dual-band filter design, particularly in the upper and lower sections of the side stubs. It is also worth noting that transmission lines, which play a key role in the final structural design, constitute essential components of stepped impedance resonators (SIRs). These resonators have recently attracted considerable attention in the design of various filters with different performance characteristics in recent research. The use of transmission lines with various architectures in the middle sections of the structure has been among the widely considered techniques to enhance performance and achieve the desired frequency. The combination of transmission line architectures with stubs and an air gap completes the design and yields the best results. The main consideration in designing the transmission line architecture lies in the middle section of the structure. Therefore, after multiple design iterations, the most optimal architecture based on frequency characteristics has been developed and presented in the final design. As shown in Fig. 11(a), by making fundamental changes to the single-band bandpass filter structure presented in Fig. 8, the proposed filter has been transformed into a dual-band bandpass filter. Among these changes that led to the dual-band bandpass filter structure are the removal of resonator T2, the addition of more resonators T3 to the middle section of the structure, adjustments to the dimensions of the middle stubs, changes in the dimensions of resonator T3, alterations in the connection point of resonator T3 to the side stubs of the structure, modifications to the dimensions of the transmission lines on the sides, and changes in the air gap between the middle stubs of resonator T3.

The designed dual-band bandpass filter has central frequencies of 7.4 GHz and 10.7 GHz. Additionally, to prevent information interference, an insertion loss of 50.4 dB is created at a specific frequency of 8.4 GHz between the two passbands, providing very good isolation between the first and second passbands. The exact dimensions of the improved structure are shown in Tab. 15. Isolation between the passbands is achieved by creating high insertion loss at the frequency between the first and second passbands. In other words, the insertion loss, which is minimum at the center frequencies of the passbands, reaches its maximum value at the isolation frequency. As such, in the design of this dual-band pass filter (as previously mentioned), this loss equals 50.4 dB. It is evident that the concept of inter-band isolation has received significant attention in recent studies. As such, given that the implemented design is a dual-band bandpass filter, the primary objective of establishing isolation between the first and second passbands is to prevent data interference. Consequently, as shown in Fig. 11(b), despite an insertion loss of 50.4 dB, this data interference has been minimized in the executed design.

In Fig. 11(b), the frequency response of the dual-band bandpass filter is shown, and the frequency characteristics of the dual-band bandpass filter EM model are presented in Tab. 16.

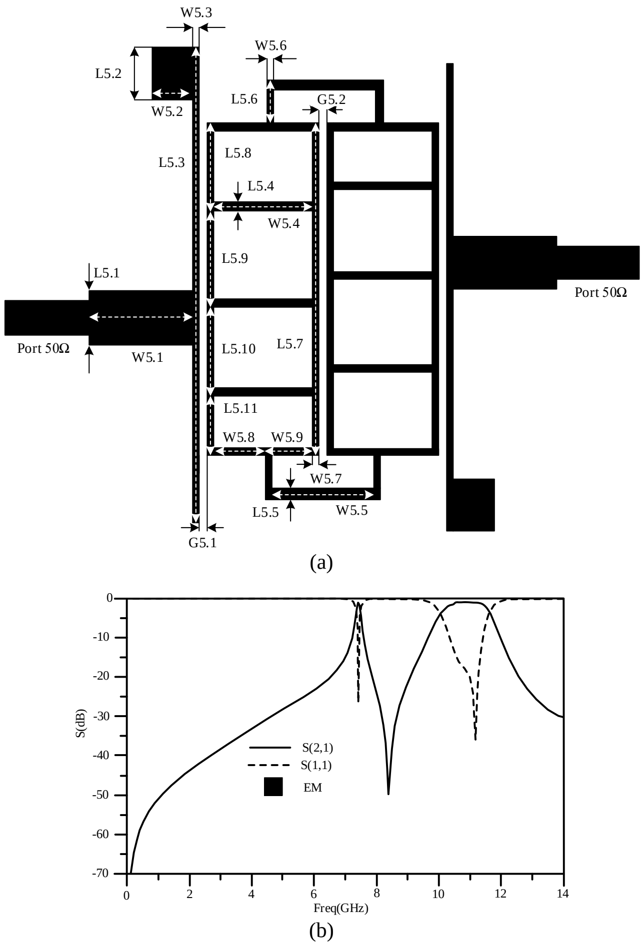

Fig. 11. (a) Structure of the dual-band bandpass filter (Design 5). (b) Filter frequency response.

Parameter	Dimension (mm)	Parameter	Dimension (mm)
W5.1	2	L5.1	1
W5.2	0.9	L5.2	1
W5.3	0.12	L5.3	6.72
W5.4	1.92	L5.4	0.14
W5.5	2	L5.5	0.2
W5.6	0.11	L5.6	0.84
W5.7	0.12	L5.7	6.17
W5.8	1.12	L5.8	1.38
W5.9	0.92	L5.9	1.68
L5.10	1.54	L5.11	1.01
G5.1	0.15	G5.2	0.15

Tab. 15. Dimensions of dual-band bandpass filter structure.

Cross band	CF (GHz)	IL (dB)	RL (dB)	FBW (%)	BW (MHz)	ISO (dB)
First	7.4	0.3	26.2	13.5	140	50.4
Second	10.7	0.9	36.1	5.79	620	

Tab. 16. Frequency response characteristics.

11. Circuit Model of the Dual-Band Bandpass Filter

Considering the fundamental changes made to the single-band filter structure that led to the enhancement of the design into a dual-band bandpass filter, these changes must be reflected in the circuit model in such a way that the frequency response of the final designed model accurately matches the electromagnetic (EM) model in terms of frequency response parameters. In Fig. 12(a), the final circuit model is presented. Table 17 provides the exact values of the calculated inductors and capacitors. In Fig. 12(b), a comparison of the frequency responses of the EM model and the circuit model is shown. The frequency response of the circuit model has a suitable match with the EM model in terms of central frequency. The calculated values of the circuit model are presented in Tab. 17. To achieve a frequency response that accurately matches the electromagnetic model, the parameters have been scanned and improved.

The frequency response specifications of the circuit model and the EM model are presented in Tab. 18.

One of the notable features in the design of balanced dual-band bandpass filters is the ability to tune parameters such as central frequency and bandwidth by making changes to the electromagnetic (EM) model. As shown in Fig. 13, in the proposed design, by changing the width of the middle stubs, the central frequency of the first passband increases from 6.9 GHz to 7.43 GHz, while the second passband decreases from 11.2 GHz to 10.73 GHz.

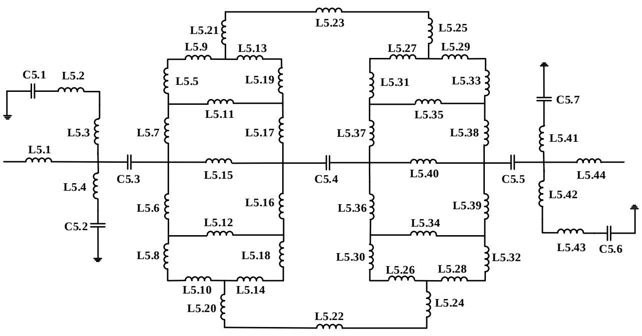

(a)

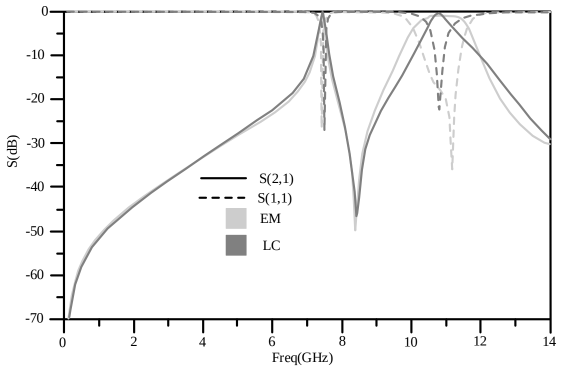

(b)

Fig. 12. (a) Circuit model of dual-band bandpass filter. (b) Comparison of frequency response of EM model and circuit model.

Element	Value	Element	Value	Element	Value
L5.1	42 nH	L5.19	5 nH	L5.25	5 nH
C5.1	0.022 pF	L5.17	5 nH	L5.20	5 nH
L5.2	0.19 nH	L5.16	5 nH	L5.22	5 nH
L5.3	2.34 nH	L5.18	5 nH	L5.24	5 nH
L5.4	1.02 nH	L5.11	2 nH	C5.7	0.015 pF
C5.2	0.015 pF	L5.15	2 nH	L5.41	1.04 nH
C5.3	0.007 pF	L5.12	2 nH	L5.42	2.32 nH
L5.7	5 nH	C5.4	0.0197 pF	L5.44	42 nH
L5.5	5 nH	L5.37	5 nH	L5.43	0.19 nH
L5.6	5 nH	L5.31	5 nH	L5.38	5 nH
L5.8	5 nH	L5.36	5 nH	L5.39	5 nH
L5.9	1.67 nH	L5.30	5 nH	L5.32	5 nH
L5.13	1.67 nH	L5.27	1.67 nH	L5.35	2 nH
L5.10	1.5 nH	L5.29	1.67 nH	L5.40	2 nH
L5.14	1.5 nH	L5.26	1.5 nH	L5.34	2 nH
L5.21	5 nH	L5.28	1.5 nH	C5.5	0.007 pF
L5.23	2 nH	L5.33	5 nH	C5.6	0.022 pF

Tab. 17. Values of dual-band bandpass filter circuit model.

Model	CF1 (GHz)	CF2 (GHz)	BW1 (MHz)	BW2 (MHz)	RL1 (dB)	RL2 (dB)	IL1 (dB)	IL2 (dB)
EM Model	7.4	10.7	140	620	26.2	36.1	0.3	0.9
Circuit Model	7.4	10.7	50	110	40.36	31.54	0.4	0.02

Tab. 18. Frequency response characteristics of the dual-band bandpass filter by both bands.

In other words, by gradually increasing the width of the middle stubs, the central frequencies of the first and second passbands become closer to each other, while the S-parameters, including insertion loss and return loss, remain within the desirable range. Table 19 displays the

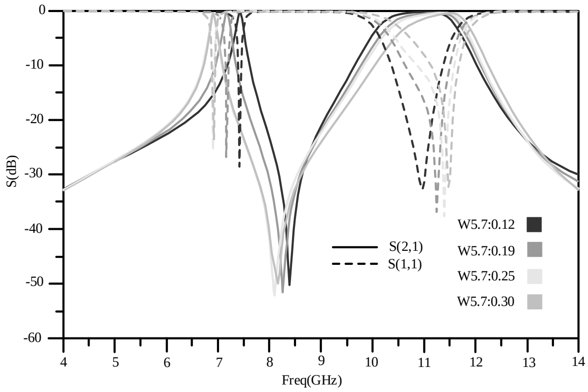

Fig. 13. Frequency response and effect of changing the width of intermediate stubs on the characteristics of the dual-band bandpass filter.

Dimension (mm)	CF1 (GHz)	CF2 (GHz)
$W = 0.3$	6.9	11.2
$W = 0.27$	6.9	11.08
$W = 0.25$	6.9	11
$W = 0.22$	7.04	10.98
$W = 0.19$	7.18	10.92
$W = 0.17$	7.25	10.86
$W = 0.15$	7.32	10.82
$W = 0.12$	7.43	10.73

Tab. 19. The effect of changing the values of the dimensions of the intermediate stubs.

exact values of the dimensions of the middle stubs and their corresponding central frequencies.

12. Fabricated Sample

The results of the fabrication and the constructed sample are shown in Fig. 14. The frequency response characteristics, delineated according to the LC model, EM

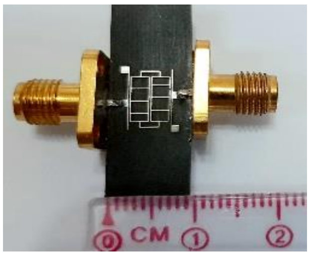

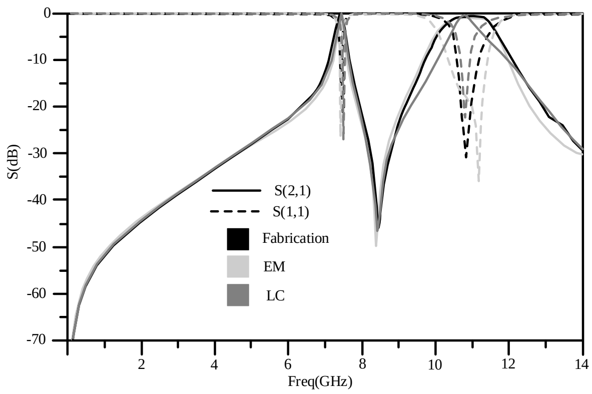

Fig. 14. Fabrication results and fabricated sample.

Model	CF1 (GHz)	CF2 (GHz)	BW1 (MHz)	BW2 (MHz)	RL1 (dB)	RL2 (dB)	IL1 (dB)	IL2 (dB)
EM Model	7.4	10.7	140	620	26.2	36.1	0.3	0.9
Circuit Model	7.4	10.7	50	110	40.36	31.54	0.4	0.02
Fabricated	7.4	10.7	110	530	22.4	31.1	1.4	2.3

Tab. 20. Frequency response characteristics.

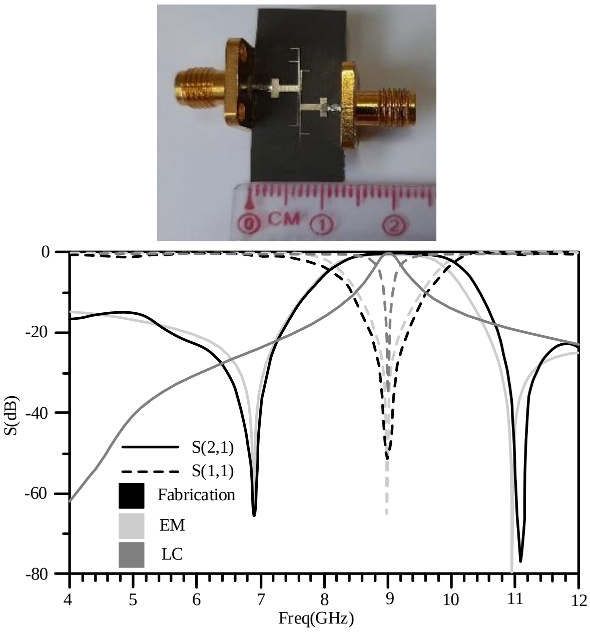

Fig. 15. Fabrication results and fabricated sample of Design 4.

model, and fabricated sample, are presented in Tab. 20. All simulations were performed using the ADS Momentum software. The substrate used is Rogers 5880 with a thickness of 15 mils, a tangent loss of 0.0009, and a dielectric constant of 2.2. Considering that today's electronics world is advancing towards compact and miniaturized devices and components, the use of this substrate leads to a reduction in the size of the resonators used and, consequently, the overall dimensions of the proposed filter.

The fabricated filter sample and the comparison between its measured, simulated, and LC model results are shown in Fig. 14 and Fig. 15. The frequency response characteristics, delineated according to the LC model, EM model, and fabricated sample, are presented in Tab. 21. Comparison of some dual-band bandpass filters, as presented in other references, along with the results of the filter designed in this paper, in terms of filter characteristics and dimensions, is provided in Tab. 22.

Model	FC (GHz)	BW(GHz)	RL (dB)	IL (dB)
EM Model	9	1.88	65.4	0.2
Circuit Model	9	0.75	34.9	0.001
Fabrication	9	1.83	54.6	1.7

Tab. 21. Frequency response characteristics.

Ref.	CF (GHz)	3-dB FBW (%)	IL (dB)	RL (dB)	Circuit Size (λ_g^2)
[1]	2.45/3.51	4.2/4.8	2.03/1.74	31/32	0.12 × 0.35
[5]	7.4/14.2	32.4/12.1	0.23/0.3	28/30	0.64 × 0.62
[9]	4.42/7.2	2.12/1.15	0.5/0.86	17.56/17.9	0.0253
[10]	5.8/13.1	58.6/20.7	0.55/1.4	35/32	0.26 × 1.35
[18]	2.13/3.47	14/11.2	0.73/0.9	32/33	0.0471
[19]	2.4/5.2	5.8/6.45	3.6/3.1	15/25	0.15 × 0.16
[20]	12/15	7/6.6	1.24/0.85	30/28	1.66 × 1.29
[21]	12/16	3.8/3.47	1.79/1.76	20/16	2.16 × 1.25
[22]	2.38/3.59	1.33/2.13	1.34/1.03	50/50	0.08 × 0.09
[23]	3.45/4.73	2.24/1.54	0.34/0.19	62/50	0.57 × 0.48
[24]	2.4/3.5	9.6/6	1.4/1.35	15.3/16.2	0.0306
[25]	2.4/3.5	9.6/7.7	1.42/1.19	25/20.1	0.482
[26]	2.3/3.2	11.3/9.4	1.1/1.7	40/12.0	0.228
[27]	2.51/5.81	19.6/10.9	0.51/1.42	45/30	0.23 × 0.23
[28]	1.64/2.37	8.86/5.69	0.92/1.94	38/31	0.24 × 0.15
[29]	2.55/3.6	20.4/5	1.22/2.13	20/18	0.21 × 0.26
[30]	3.78/4.82	11.3/10.7	1.38/1.72	15/30	0.0496
[31]	1.8/5.8	8.7/5.4	1.2/2.0	35/26	0.37 × 0.38
[32]	2.6/5.8	10.4/3.6	1.1/2.15	20/16	0.26 × 0.34
[33]	2.0/2.7	7.5/5.4	2.2/2.5	18/20	0.2 × 0.13
[34]	2.5/5.6	6.5/3.0	1.06/2.04	30/23	0.15 × 0.26
[35]	9.23/14.05	2.8/5.6	2.9/2.7	21/28	2.7 × 1.27
[36]	3.58/5.6	5.8/3.4	1.1/1.8	30/22	0.25 × 0.47
This work	**7.4/10.7**	**13.5/5.79**	**1.4/2.3**	**22.4/31.1**	**0.16 × 0.23**

Tab. 22. Comparison of some previous dual-band bandpass filters.

13. Conclusions

In this paper, a tunable dual-band microstrip bandpass filter based on stepped impedance resonators (SIR) has been designed and presented. The design process was carried out in stages, starting with the basic design created using a stepped impedance resonator. This research involved enhancing the basic design through various structural modifications. These improvements included fundamentally rearranging the basic structure by moving the side stubs to the central section, optimizing the dimensions of the transmission lines and middle stubs, precisely adjusting the air gap between the central stubs, and adding resonators T1, T2, and T3. Additionally, the combination of the designed single-band filter structures was performed to achieve a balanced dual-band bandpass filter. In the design process, after applying modifications and optimizing the electromagnetic model (EM) structure at each stage, the corresponding circuit model (CM) was also designed, and the frequency responses of both models were compared and evaluated. Finally, the results obtained from the electromagnetic model (EM) simulation, the circuit model (CM), and the fabricated physical sample were compared, showing significant consistency.

References

[1] LIU, X., REN, B., GUAN, X., et al. High selectivity dual-band balanced BPF with controllable passbands based on magnetically coupled capacitor-loaded SIRs. *IEEE Transactions on Circuits and Systems II: Express Briefs*, 2023, vol. 70, no. 9, p. 3293–3297. DOI: 10.1109/TCSII.2023.3271152

[2] ZAKHAROV, A., ROZENKO, S., LITVINTSEV, S. Transmission line loop resonators short-circuited in middle. *IEEE Transactions on Circuits and Systems II: Express Briefs*, 2022, vol. 69, no. 4, p. 2006–2010. DOI: 10.1109/TCSII.2021.3138937

[3] LUO, X., CHENG, X., JIANG, J., et al. Miniaturized millimeter-wave dual-band band-pass on-chip filter in 0.13-μm SiGe BiCMOS. *AEU - International Journal of Electronics and Communications*, 2025, vol. 189, p. 1–9. DOI: 10.1016/j.aeue.2024.155591

[4] İSCAN, E., DURGUN, A. C. A tunable bandpass filter using substrate integrated waveguide resonator. *AEU - International Journal of Electronics and Communications*, 2025, vol. 197, p. 1 to 9. DOI: 10.1016/j.aeue.2025.155814

[5] MUSHTAQ, B., KHALID, S. Design of miniaturized single and dual-band bandpass filters using diamond-shaped coupled line resonator for next-generation wireless systems. *International Journal of Microwave and Wireless Technologies*, 2023, vol. 15, no. 3, p. 375–383. DOI: 10.1017/S1759078722001416

[6] LA, D. S., WANG, M. Y., ZHANG, Y. J., et al. A cylindrical cavity differential dual-band bandpass filter (DDBBPF) with stepped cylinders. *AEU - International Journal of Electronics and Communications*, 2022, vol. 155, p. 1–8. DOI: 10.1016/j.aeue.2022.154358

[7] CASTRO, N., PIZARRO, F., HERRÁN-ONTANÓN, L. F., et al.. Evaluation of inverted microstrip gap waveguide bandpass filters for Ka-band. *AEU - International Journal of Electronics and Communications*, 2021, vol. 134, p. 1–6. DOI: 10.1016/j.aeue.2021.153677

[8] WEI, F., ZHANG, C. Y., ZENG, C., et al. A reconfigurable balanced dual-band bandpass filter with constant absolute bandwidth and high selectivity. *IEEE Transactions on Microwave Theory and Techniques*, 2021, vol. 69, no. 9, p. 4029–4040. DOI: 10.1109/TMTT.2021.3093907

[9] LALBAKHSH, A., GHADERI, A., MOHYUDDIN, W., et al. A compact C-band bandpass filter with an adjustable dual-band suitable for satellite communication systems. *Electronics*, 2020, vol. 9, no. 7, p. 1–17. DOI: 10.3390/electronics9071088

[10] JIANG, Y., HUANG, L., HUANG, Z., et al. Compact wideband dual-band SIW bandpass filters. *Applied Computational Electromagnetics Society Journal*, 2021, vol. 36, no. 9, p. 1254 to 1259. DOI: 10.47037/2021.ACES.J.360919

[11] MOITRA, S., DEY, R. Design of dual band and tri band bandpass filter (BPF) with improved inter band isolation using DGS integrated coupled microstrip lines structures. *Wireless Personal Communications*, 2019, vol. 110, p. 2019–2030. DOI: 10.1007/s11277-019-06827-8

[12] FERNÁNDEZ-PRIETO, A., MARTEL, J., UGARTE-PARRADO, P. J., et al. Compact balanced dual-band bandpass filter with magnetically coupled embedded resonators. *IET Microwaves, Antennas & Propagation*, 2019, vol. 13, no. 4, p. 492–497. DOI: 10.1049/iet-map.2018.5573

[13] XU, Z., XU, J. Design of dual-mode filters using stepped impedance resonators with stub loading. In *2012 International Conference on Microwave and Millimeter Wave Technology (ICMMT)*. Shenzhen (China), 2012, vol. 4, p. 1–3. DOI: 10.1109/ICMMT.2012.6230282

[14] MEESOMKLIN, S., CHOMTONG, P., AKKARAEKTHALIN, P. A compact multiband BPF using step-impedance resonators with interdigital capacitors. *Radioengineering*, 2016, vol. 25, no. 2, p. 258–267. DOI: 10.13164/re.2016.0258

[15] LOTFI, S., ROSHANI, S., ROSHANI, S., et al. Compact microstrip balanced bandpass filter with stepped impedance resonator for wireless application. In *2024 International Conference on Applied Electronics (AE)*. Pilsen (Czech Republic) 2024, p. 1–4. DOI: 10.1109/AE61743.2024.10710284

[16] LI, S., LI, S., YUAN, J. A compact fourth-order tunable bandpass filter based on varactor-loaded step-impedance resonators. *Electronics*, 2023, vol. 12, no. 11, p. 1–14. DOI: 10.3390/electronics12112539

[17] HONG, J.-S., LANCASTER, M. J. *Microstrip Filters for RF/Microwave Applications*. New York: Wiley, 2001. ISBN: 9780471388777

[18] HOU, Z., LIU, C., ZHANG, B., et al. Dual-/tri-wideband bandpass filter with high selectivity and adjustable passband for 5G mid-band mobile communications. *Electronics*, 2020, vol. 9, no. 2, p. 1–13. DOI: 10.3390/electronics9020205

[19] XU, S., MA, K., MENG, F., et al. Novel defected ground structure and two-side loading scheme for miniaturized dual-band SIW bandpass filter designs. *IEEE Microwave and Wireless Components Letters*, 2015, vol. 25, no. 4, p. 217–219. DOI: 10.1109/LMWC.2015.2400916

[20] ZHOU, K., ZHOU, C.-X., WU W. Substrate-integrated waveguide dual-mode dual-band bandpass filters with widely controllable bandwidth ratios. *IEEE Transactions on Microwave Theory and Techniques*, 2017, vol. 65, no. 10, p. 3801–3812. DOI: 10.1109/TMTT.2017.2694827

[21] ZHOU, K., ZHOU, C.-X., WU, W. Resonance characteristics of substrate-integrated rectangular cavity and their applications to dual-band and wide-stopband bandpass filters design. *IEEE Transactions on Microwave Theory and Techniques*, 2017, vol. 65, no. 5, p. 1511–1524. DOI: 10.1109/TMTT.2016.2645156

[22] SONG, Y., LIU, H., ZHAO, W., et al. Compact balanced dual-band bandpass filter with high common-mode suppression using planar via-free CRLH resonator. *IEEE Microwave and Wireless Components Letters*, 2018, vol. 28, no. 11, p. 996–998. DOI: 10.1109/LMWC.2018.2873240

[23] SONG, Y., LIU, H., FENG, L., et al. High-order balanced dual-band HTS BPF with flexible frequency ratio and sharp rejection skirts. *IEEE Transactions on Microwave Theory and Techniques*, 2022, vol. 70, no. 4, p. 2185–2195. DOI: 10.1109/TMTT.2022.3148420

[24] CHEN, F. C., CHU, Q. X., TU, Z. H. Design of compact dual-band bandpass filter using short stub loaded resonator. *Microwave and Optical Technology Letters*, 2009, vol. 51, no. 4, p. 959–963. DOI: 10.1002/mop.24209

[25] DENIS, B., SONG, K., ZHANG, F. Compact dual-band bandpass filter using open stub-loaded stepped impedance resonator with cross-slots. *International Journal of Microwave and Wireless Technologies*, 2017, vol. 9, no. 2, p. 269–274. DOI: 10.1017/S1759078715001786

[26] LI, K., KANG, G.-Q., LIU, H., et al. High-selectivity adjustable dual-band bandpass filter using a quantic-mode resonator. *Microsystem Technologies*, 2020, vol. 26, no. 3, p. 913–916. DOI: 10.1007/s00542-019-04616-8

[27] DONG, G., WANG, W., WU, Y., et al. Dual-band balanced bandpass filter using slotlines loaded patch resonators with independently controllable bandwidths. *IEEE Microwave and Wireless Components Letters*, 2020, vol. 30, no. 7, p. 653–656. DOI: 10.1109/LMWC.2020.2995963

[28] MEDRAN DEL RIO, J. L., LUJAMBIO, A., FERNÁNDEZ-PRIETO, A., et al. Multi-layered balanced dual-band bandpass filter based on magnetically coupled open-loop resonators with intrinsic common-mode rejection. *Applied Sciences*, 2020, vol. 10, no. 9, p. 1–13. DOI: 10.3390/app10093113

[29] ZHU, C., XU, J., ZHANG, G., et al. Split-type dual-band bandpass filters with symmetric/asymmetric response. *IEEE Microwave and Wireless Components Letters*, 2017, vol. 28, no. 1, p. 25–27. DOI: 10.1109/LMWC.2017.2776931

[30] WANG, L.-T., XIONG, Y., GONG, L., et al. Design of dual-band bandpass filter with multiple transmission zeros using transversal signal interaction concepts. *IEEE Microwave and Wireless Components Letters*, 2018, vol. 29, no. 1, p. 32–34. DOI: 10.1109/LMWC.2018.2884147

[31] WU, X., WAN, F., GE, J. Stub-loaded theory and its application to balanced dual-band bandpass filter design. *IEEE Microwave and Wireless Components Letters*, 2016, vol. 26, no. 4, p. 231–233. DOI: 10.1109/LMWC.2016.2537045

[32] REN, B., LIU, H., MA, Z., et al. Compact dual-band differential bandpass filter using quadruple-mode stepped-impedance square ring loaded resonators. *IEEE Access*, 2018, vol. 6, p. 21850 to 21858. DOI: 10.1109/ACCESS.2018.2829025

[33] FU, S., WU, B., CHEN, J., et al. Novel second-order dual-mode dual-band bandpass filters using capacitance loaded square loop resonator. *IEEE Transactions on Microwave Theory and Techniques*, 2012, vol. 60, no. 3, p. 477–483. DOI: 10.1109/TMTT.2011.2181859

[34] BAGCI, F., FERNÁNDEZ-PRIETO, A., LUJAMBIO, A., et al. Compact balanced dual-band bandpass filter based on modified coupled-embedded resonators. *IEEE Microwave and Wireless Components Letters*, 2017, vol. 27, no. 1, p. 31–33. DOI: 10.1109/LMWC.2016.2629962

[35] SHEN, Y., WANG, H., KANG, W., et al. Dual-band SIW differential bandpass filter with improved common-mode suppression. *IEEE Microwave and Wireless Components Letters*, 2015, vol. 25, no. 2, p. 100–102. DOI: 10.1109/LMWC.2014.2382683

[36] ZHOU, L.-H., CHEN, J.-X. Differential dual-band bandpass filters with flexible frequency ratio using asymmetrical shunt branches for wideband CM suppression. *IEEE Transactions on Microwave Theory and Techniques*, 2017, vol. 65, no. 11, p. 4606–4615. DOI: 10.1109/TMTT.2017.2700275

About the Authors ...

Morteza KHAJAVI received the B.Eng. and M.Eng. degrees in Electronics Engineering from Jundi-Shapur University of Technology, Dezful, Iran, in 2017 and 2019, respectively. He is currently working toward the Ph.D. degree in Electrical Engineering at Shahid Chamran University of Ahvaz, Ahvaz, Iran. His research interests include analog and radio-frequency (RF) circuit design.

Ebrahim FARSHIDI (corresponding author) was born in Shoushtar, Iran, in 1973. He received the B.Sc. degree in 1995 from Amir Kabir University of Technology, Tehran, Iran, the M.Sc. degree in 1997 from Sharif University of Technology, Tehran, Iran and the Ph.D. degree in 2008 from IUT, Esfahan, Iran, all in Electronic Engineering. He worked for Karun Pulp and Paper Company during 1997–2002. From 2002 he has been with Shahid Chamran University, Ahvaz, Iran, where he is currently Professor of Electrical Engineering Department. His areas of interest include current-mode circuits design, and data converters. He is author of more than 85 technical papers in electronics.

Mohammad SOROOSH received B.Eng. degree from Isfahan University of Technology at Isfahan in 2000 and M.Eng. and Ph.D. degrees from Tarbiat Modares University at Tehran in 2003 and 2009, respectively, all in Electronics. He joined Iran Telecommunication Research Center, Tehran in 2003 where he was a researcher at optical communication group. Currently, he is a Professor of Electronics at Shahid Chamran University of Ahvaz. His expertise is further evidenced by his selection as a top 2% scientist in 2023, 2024 and 2025. His research interests are in modeling and simulation of photonic and optoelectronic devices.

Shahrzad AJABI received the B.Sc. degree from Sharif University of Technology, Tehran, Iran, in 1998, and M.Sc. degree from Tarbiat Modares University, Tehran, Iran, in 2002, both in Telecommunication Engineering. She joined the Department of Electrical Engineering, Shahid Chamran University of Ahvaz, Iran, in 2018, as an Assistant Professor. Her research interests include analog and RF circuits.